THERMO ELASTO-PLASTIC CONTACT ANALYZIS FOR HIGH TEMPERATURE APPLICATIONS

by

Samir DANOUNI[a,b]*, Shayfull ZAMREE ABD RAHIM[c,d], Abdellah ABDELLAH EL-HADJ[a], and Mohd Nasir MAT SAAD[c,d]

[a] Laboratory of Mechanics, Physics and Mathematical Modelling (LMP2M), University of Medea, Medea, Algeria
[b] University Center of Tipaza, Tipaza, Algeria
[c] Green Design and Manufacture Research Group, Center of Excellence Geopolymer and Green Technology (CEGeoGTech), Universiti Malaysia Perlis, Kangar, Perlis, Malaysia
[d] School of Manufacturing Engineering, Universiti Malaysia Perlis, Kampus Tetap Pauh Putra, Arau, Perlis, Malaysia

Original scientific paper
https://doi.org/10.2298/TSCI201026276D

This study presents the development of a thermo-mechanical simulation model for an elastic-plastic contact problem between a half cylinder and a plane plate. The set of equations was solved using direct coupling method by ANSYS mechanical. The results obtained from the present numerical model of the structural contact without heat transfer are compared with those of analytical, experimental and other numerical models. Then, the contact problem was solved using a coupled thermo-mechanical model. Computational results showed significant effects of thermal consideration in the elastic-plastic contact problem. Large deformations of structure due to high temperature are predicted using the thermo-mechanical model with elastic-plastic deformations. This model is useful to predict deformations on the structural components due to contact at high temperature situation.

Key words: *thermo-mechanical, elastic-plastic model, finite element analyzis, surface-surface contact*

Introduction

The contact between parts is an important phenomenon in most mechanical designs, such as electrical contacts, bolted connections, heat exchanger tubes in nuclear application, data storage devices, micro- and nanoscale applications, machining, rollers and bearing, brake disks, and other applications [1-9]. There are some researchers that studied the thermomechanical contact between aluminum and steel for high temperature applications [10-12]. Among, we cite the impact and the spreading out of the particles of aluminum on the steel substrate during thermal spraying [13, 14], the study of the interface workpieces/tooling during the aluminum extrusion [15], and other applications [16, 17].

The contact is a strong non-linearity due to the normal and the tangential stiffness at the inter surfaces which changes significantly with the changing of contact status [18-21]. The formulation named the Hertz's contact between two bodies in the elastic state has been devel-

* Corresponding author, e-mail: abdellah_elhadj.a@gmail.com

oped, which effectively describes the relation of contact force-displacement in the case of small deformation (contact strain less than 1%) [22]. However, the stresses of the contact may lead to plastic deformation. Several researchers studied the problem of the mechanical contact between two bodies in the elastic phase [23-28]. Due to the non-linearity of the material behavior with plastic deformations, the experimental methods and the numerical calculations are used to determine the material deformation. In this situation, the correct characterization of the mechanical behavior of the material is crucial. The detection of the curve of deformation with exactitude requires the modeling of several parameters [29-36].

At high temperature applications, the heat transfer due to temperature variation has a significant effect on the material properties [37, 38]. Thermomechanical contact was studied with elastical behavior [24, 39]. Authors have analyzed the effects of high temperature and high pressure on stress-strain distribution. On the other hand, Danouni *et al.* [40] studied a thermo-elastoplastic model of the impact of a spherical particle in order to predict coating formation during thermal spraying. A coupled mechanical and energy equations are solved using numerical methods. It is noticed that thermal effects have a crucial role in contact behavior [41-43]. Instead of using a perfect concept of contact, authors have used the correlation of thermal contact conductance (TCC) [42] to model the structural-thermal contact.

Problem statement

Based on authors' knowledge, the previous researchers did not study a multiphysical problem which treats a contact between two mechanical parts for elastoplastic behavior with taking into account the heat transfer between them, and the influence of the temperature on its mechanical characteristics. Consequently, it is important to study the correlation between elasto-plastic contact and thermal effects for high temperature applications. In this work, thermomechanical analyzis in elasto-plastic regime using a coupled field strategy was performed. First of all, a static contact between an aluminum half cylinder and a steel plate is considered. In order to validate the model developed in this study, a comparison of present model with experimental and numerical results of Doca and Andrade Pires [32] was made. In this case, the elastic-plastic contact of two bodies are treated without temperature variation and the effect of TCC is not included. Then, an empirical formula of the TCC dependent of the pressure and the temperature on the level of the contact was employed. The results are drawn for elasto-plastic domain to illustrate the importance of heat transfer in contact problems which is useful to predict deformations on the structural components due to contact at high temperature situation.

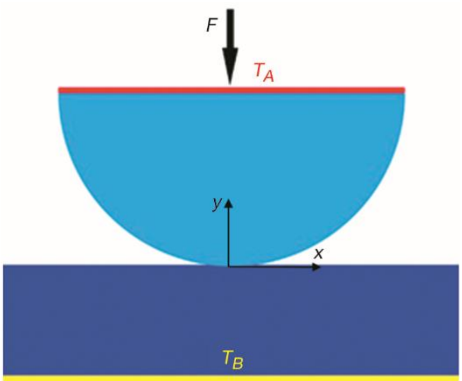

Figure1. The physical domain; *F* [N] is the applied force, *TA* and *TB* [K] are temperatures of top surface of the half cylinder and the bottom surface of the plate, respectively

Mathematical modeling

A finite element method was employed in this study for a non-linear elasto-plastic contact problem. The numerical simulation tests were executed by ANSYS parametric design language (APDL). The physical domain is illustrated in fig. 1. The aluminum half cylinder has a radius of 20 mm, while the mild steel flat plate has the dimensions of 60 × 20 mm and a thickness of 20 mm. The vertical force, *F*, is exerted on the upper surface of the half cylinder. The *TA* and *TB* are temperatures of top surface of the half cylinder and the bottom surface of the plate, respectively. The material properties of these two bodies are temperature dependent as tabulated in tab. 1.

Table 1. Material properties as function of temperature [3]

Properties	Young modulus [GPa]		Tangent modulus [MPa]		Yielding stress [MPa]		Thermal conductivity [Wm^{-1}K^{-1}]		Thermal expansion 10^{-6} [K^{-1}]	
Mild steel	T [°C]	E	T [°C]	ET	T [°C]		T [°C]	K	T [°C]	α
density	21	207.6	21	2076	21	248	21	64.8	21	11
ρ = 7800 kg/m^3	93	207.6	93	1964	93	238	93	63.31	93	11.5
Poisson	204	194	204	…	204	224	204	55.38	204	12.2
coefficient	316	186	316	1860	316	200	316	49.99	316	13
ν = 0.303	427	169	427	1690	427	172	427	44.9	427	13.5
C_p = 500 [Jkg^{-1}K^{-1}]	538	117	538	…	538	145	538	39.81	538	14
Aluminum	T [°C]	E	T [°C]	ET	T [°C]		T [°C]	K	T [°C]	α
density	20	69.3	21	345	20	178.5	21	178	20	22.7
ρ = 2700 kg/m^3	100	65.6	93	…	100	…	93	180.73	100	22.8
Poisson	200	59.2	204	103	200	142,5	204	185.16	200	23.5
coefficient	300	49.7	316	34.5	300	81.1	316	188.52	300	24.7
ν = 0.35	400	30.2	427	15	400	25.3	427	184.11	400	25.7
C_p = 890 [Jkg^{-1}K^{-1}]	500	10.9	538	1.5	500	5.7	538	179	500	26.9

Hertizian model

An analytical model based on Hertz's theory is used to determine the analytical values of the width of the contact, *b*, and the maximum pressure, P_{Cmax}. According to the theory of elasticity [1], the values of *b* and P_{Cmax} (the pressure located at center point, P_0) are calculated by:

$$b = \sqrt{\frac{2Fd}{\pi l E^*}} \tag{1}$$

$$P_0 = \frac{2F}{\pi b l} \tag{2}$$

where *F* [N] is the applied force, *l* and *d* [mm] – the length and the diameter of the cylinder, respectively, *b* [mm] – the contact radius, P_0 [MPa] – the maximum pressure located at center point, and E^* is the equivalent elastic modulus [1].

The pressure profile along contact line is assumed to be parabolic [1]:

$$p(x) = P_0 \sqrt{1 - \left(\frac{x}{b}\right)} \tag{3}$$

Thermo-mechanical model

Stress equilibrium equation can be simplified in 2-D:

$$\sigma_{ij,i}(x,y) + f_i = 0 \quad i, j = 1, 2 \tag{4}$$

where σ_{ij} are cartesian component of stress tensor and f_i – the external forces applied to the system. The total strain tensor $\{\varepsilon\}$ is:

$$\{\varepsilon\} = \{\varepsilon^e\} + \{\varepsilon^p\} + \{\varepsilon^{th}\} \tag{5}$$

where $\{\varepsilon^e\}$ is the elastic strain, $\{\varepsilon^p\}$ – the plastic strain, and $\{\varepsilon^{th}\}$ – the thermal strain.

For small values of stresses, material is elastic. However, the plasticity occurs when the material is loaded beyond its yield strength. Yield criterion (Von-Misses) determines where yielding of material will occur, and it is expressed [44]:

$$\phi = \sigma_\mathrm{e} - \sigma_\mathrm{y} \tag{6}$$

where ϕ is the yield function, σ_y – the yield strength, and σ_e – the effective stress.

The displacement of the yield surface is described by flow rule (plastic straining). The yield surface depends on the increment of plastic strain [44]:

$$d\epsilon^P = \lambda \left\{ \frac{\partial Q}{\partial \sigma} \right\} \tag{7}$$

where λ is the plastic multiplicator which represents the plastic deformation magnitude.The direction of plastic straining is expressed by the gradient of the plastic potential $\{\partial Q/\partial\sigma\}$.

In this study, isotropic hardening behavior models are considered. A small strain deformation is assumed in this situation. Consistency states that, during hardening, stress should always lie on the yield surface, which is given by the following condition [44]:

$$\mathrm{d}F = \left\{ \frac{\partial F}{\partial \sigma} \right\}^T \mathrm{d}\sigma + \left\{ \frac{\partial F}{\partial \epsilon^{PL}} \right\}^T \mathrm{d}\epsilon^P = 0 \tag{8}$$

The structural strains change the density of entropy, thus directly influence the internal energy of the structure. The density of entropy, S, is given by [44]:

$$S = \{\alpha\}^T \{\sigma\} + \frac{\rho C_P}{T_0} \Delta T \tag{9}$$

where T_0 is an absolute reference temperature, α – the thermal expansion coefficient, C_p – the specific heat at constant stress, and ρ – the density. It is considered that all the processes exerted on materials are reversible, and the second law of thermodynamics was applied.

The static thermal model given by the law of Fourier for the heat transfer by conduction, and integrated with the conservation energy equation (First law of thermodynamics):

$$\nabla^T \left(k \nabla T \right) + G = 0 \tag{10}$$

where k and G are the thermal conductivity and the heat source, respectively.

The contact heat transfer between the half cylinder and the plate is predicted by [40]:

$$q_\mathrm{F} = TCC(T_\mathrm{C} - T_\mathrm{t}) \tag{11}$$

where q_F is the density of heat flux, T_C – the contact temperature, and T_t – the target temperature. In this work, an emperical correlation based on an Hertzian theory to calculate the *TCC* is used [40]:

$$TCC = 1.9 \frac{k_s}{\sigma_\mathrm{r}} \left(\frac{P_\mathrm{C}}{E^*} \right)^{0.94} \tag{12}$$

where k_s is the equivalent thermal conductivity of the contact $2k_1k_2/(k_1 + k_2)$. The surface roughness is estimated by σ_r. The contact pressure P_C is set to be $(2/3)P_0$, where P_0 is calculated from eq. (2). The E^* is obtained for the temperature T_C. The *TCC* values as a function of T_C and P_C are given in tab. 2.

Table 2. Calculated *TCC* values for al-steel contact obtained from eq. (12)

T_C [°C] / P_C [Pa]	20	100	200	300	400	500
1	$1.35\cdot10^{-02}$	$1.38\cdot10^{-02}$	$1.39\cdot10^{-02}$	$1.49\cdot10^{-02}$	$2.04\cdot10^{-02}$	$4.4912\cdot10^{-02}$
$1.00\cdot10^{01}$	$1.17\cdot10^{-01}$	$1.20\cdot10^{-01}$	$1.21\cdot10^{-01}$	$1.30\cdot10^{-01}$	$1.78\cdot10^{-01}$	$3.9116\cdot10^{-01}$
$1.00\cdot10^{02}$	$1.02\cdot10^{00}$	$1.05\cdot10^{00}$	$1.05\cdot10^{00}$	$1.13\cdot10^{00}$	$1.55\cdot10^{00}$	$3.4069\cdot10^{00}$
$1.00\cdot10^{03}$	$8.91\cdot10^{00}$	$9.10\cdot10^{00}$	$9.18\cdot10^{00}$	$9.85\cdot10^{00}$	$1.35\cdot10^{01}$	$2.9700\cdot10^{01}$
$1.00\cdot10^{04}$	$6.08\cdot10^{01}$	$7.93\cdot10^{01}$	$8.00\cdot10^{01}$	$8.58\cdot10^{01}$	$1.17\cdot10^{02}$	$2.5800\cdot10^{02}$
$1.00\cdot10^{05}$	$6.76\cdot10^{02}$	$6.90\cdot10^{02}$	$6.97\cdot10^{02}$	$7.47\cdot10^{02}$	$1.02\cdot10^{03}$	$2.2509\cdot10^{03}$
$1.00\cdot10^{06}$	$5.89\cdot10^{03}$	$6.01\cdot10^{03}$	$6.07\cdot10^{03}$	$6.51\cdot10^{03}$	$8.91\cdot10^{03}$	$1.9605\cdot10^{04}$
$1.00\cdot10^{07}$	$5.13\cdot10^{04}$	$5.24\cdot10^{04}$	$5.28\cdot10^{04}$	$5.67\cdot10^{04}$	$7.76\cdot10^{04}$	$1.7075\cdot10^{05}$
$1.00\cdot10^{08}$	$4.47\cdot10^{05}$	$4.56\cdot10^{05}$	$4.60\cdot10^{05}$	$4.94\cdot10^{05}$	$6.76\cdot10^{05}$	$1.4872\cdot10^{06}$
$1.00\cdot10^{09}$	$3.89\cdot10^{06}$	$3.97\cdot10^{06}$	$4.01\cdot10^{06}$	$4.30\cdot10^{06}$	$5.88\cdot10^{06}$	$1.2953\cdot10^{07}$
$1.00\cdot10^{10}$	$3.39\cdot10^{07}$	$3.46\cdot10^{07}$	$3.49\cdot10^{07}$	$3.74\cdot10^{07}$	$5.12\cdot10^{07}$	$1.1281\cdot10^{08}$

Coupled finite element method

The mesh of the geometry used in this work is illustrated in fig. 2. Plane 223 element type of ANSYS is used to analyze a coupled thermal-structural problem. The contact was modeled using two elements (Conta172 and Targe 169) called surface to surface elements [45]. All nodes of the lower surface of plate are fixed.

A mesh independence study was done, in which, we calculated the pressure and the width of the contact for different meshes. An optimal mesh is obtained, which a better precision with a reduced computation time. The mesh applied to the geometry used in this work is composed of 10770 elements and 36613 nodes.

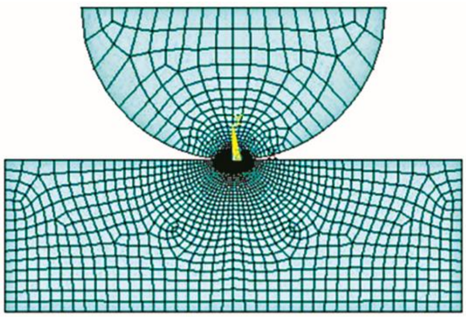

Figure 2. Mesh of the physical domain

Plane 223 also includes thermoplastic effect whereby some of the plastic work are converted to heat which results in temperature increment. In this problem, the heat equation and stress equation of motion are also coupled by the plastic heat density rate, $\dot{Q}^P$ given by [45]:

$$\dot{Q}^P = \gamma \dot{W}^P \tag{13}$$

where γ is a ratio of plastic work and $\dot{W}^P$ dissipated to heat. The plastic work is given by:

$$\dot{W}^P = \{\sigma\}\{\varepsilon^P\} \tag{14}$$

An iterative method with direct coupling was used whereby the temperature field and displacements can be obtained using the following solution [45]:

$$\begin{bmatrix} [k] & \lfloor k^{ut} \rfloor \\ [0] & \left[k^t\right] \end{bmatrix} \begin{Bmatrix} \{u\} \\ T \end{Bmatrix} = \begin{Bmatrix} \{F\} \\ \{Q\} + \{Q^P\} \end{Bmatrix} \tag{15}$$

The element matrix $[k]$ represents the stiffness effect. The force $\{F\}$ represents the nodal force in the element, while $[kt]$ is the diffusion conductivity matrix element. The element matrix $[kut]$ takes into account the thermos-elastic stiffness effect. The element vector $\{Q\}$ represents the effect of the heat generation and convection heat flow. Finally, $\{Q^P\}$ is the element plastic heat generation rate load.

Results and discussion

To validate the numerical model developed in this study, a comparison is made between the analytical solutions and results obtained by Doca and Andrade Pires [32]. The comparisons are done first, in the elastic strain state, then, in the plastic strain state. After that, results using a thermo-mechanical model were obtained for the elastic-plastic behavior which included the effects of the temperature using the *TCC* parameter on the contact.

Numerical model validation

The results of an aluminum (half cylinder) in contact with tungsten plate during the elastic stage were investigated [27]. Three values of force were used in this study: 0.1 kN, 0.2 kN, and 0.3 kN. First, results obtained for the contact width, tab. 3 showed a good agreement with the analytical model and Doca and Andrade Pires [32]. The analytical results are obtained by Hertz model using eqs. (1) and (2).

Table 3. Results in elastic domain

F_N [KN]	b [mm]					P_{Cmax} [MPa]			
	Analyt	Experimental [32]	Numerical [32]	Present model		Analyt	Experimental [32]	Numerical [32]	Present model
0.1	0.042	0.043	0.041	0.042		75.45	75.69	76.00	71.5
0.2	0.059	0.061	0.066	0.063		106.70	107.12	107.77	101.18
0.3	0.073	0.074	0.078	0.076		130.68	133.33	131.58	124

However, for the contact pressure results, there is a difference between the present numerical model developed in this study and theoretical models. This difference is due to the fact that, the analytical model assumes a parabolic curve, eq. (3), with maximum value P_0. Doca and Andrade Pires [32] used the same equation, eq. (3), where P_0 is calculated by F/AC (AC is the area of the zone of the contact). However, the curve of contact pressure obtained by finite element method in the model developed in this study is not parabolic which seems to be more realistic. The maximum point, P_{Cmax}, is situated exactly at the center point as illustrated in fig. 3. The value of maximum pressure is function of applied force. In addition, it can be noticed that, the increase of the applied force causes the increase of the contact pressure.

The Hertzian method was not used for the mode of plastic strain because it does not yield credible results. Thus, the results from the model obtained in this study was compared to the experimental results presented by Doca and Andrade Pires [32].

The maximum contact pressure from the experimental works done by Doca and Andrade Pires [32] was compared to the model developed in this study, fig. 4. The maximum pressure in experimental was calculated using eq. (2), assuming a parabolic curve [32]. However, this is true for the elastic domain (Hertz model). For the plastic domain, the maximum contact pressure do not follow a parabolic curve as presented in fig. 5. The contact pressure increases until the body reaches the plastic state. In this situation, the energy was dissipated in the plastic regime. The curve is practically parabolic for the low applied forces and becomes flattened for the high applied forces. The shape of the contact pressure indicates the function of the applied force as compared to the analytical solution which adopted an unfounded parabolic shape for all cases.

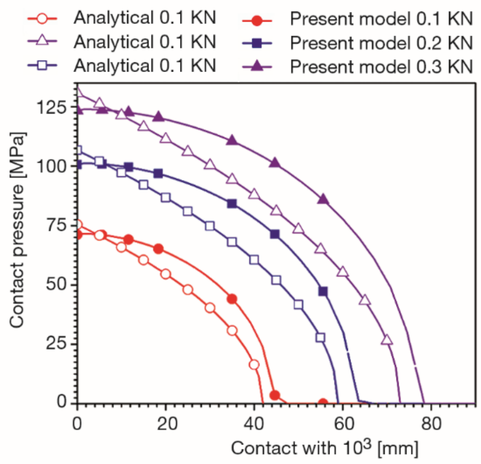

Figure 3. Contact pressure along half-contact width

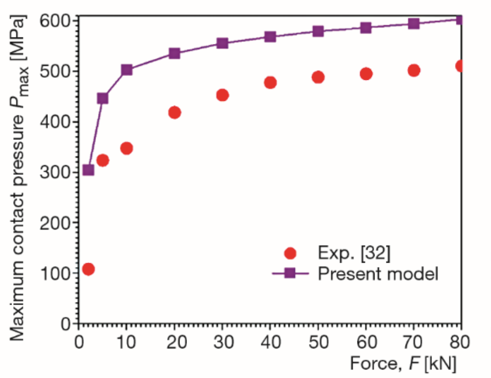

Figure 4. Miso model for elastic-plastic behavior; (a) multilinear stress-strain curves and (b) maximum contact pressure

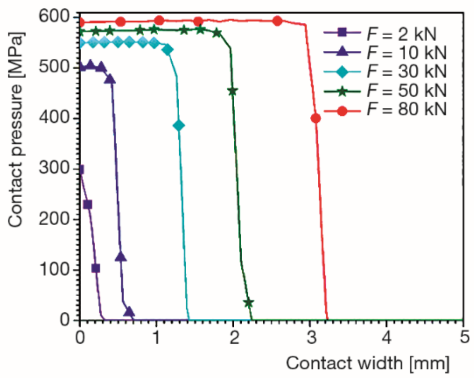

Figure 5. Contact pressure along half-contact width

Elastic-plastic thermomechanical simulation

A thermomechanical model, which considers the thermal effects during the deformation, is employed to model the elastic-plastic contact for the case of TA = 125 °C and TB = 25 °C. Figure 6 shows the temperature contours for two applied forces. From fig. 6, it can be seen that the heat transfer is proportional to the contact width, which is dependent on the force applied. The heat transfer was improved with the increase of applied forces. Plastic strain contours are illustrated in fig. 7. The plastic strain on the cylinder starts at the contact zone. The affected zone increases with the increase of the applied force.

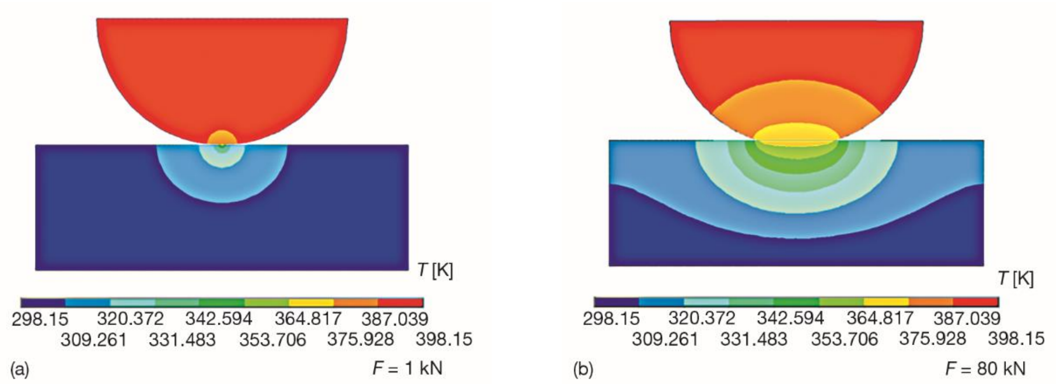

Figure 6. Temperature of elastic-plastic contact of temperature gradient for *TA* = 125 °C and *TB* = 25 °C

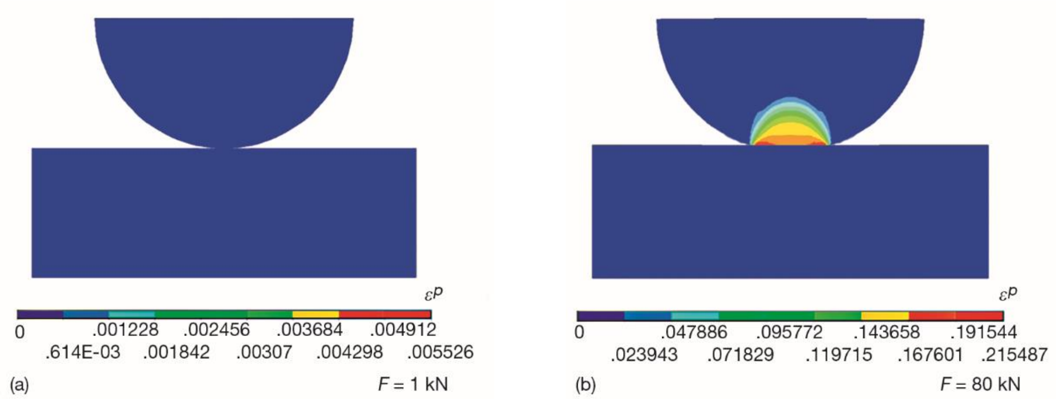

Figure 7. Plastic strain of elastic-plastic contact for *TA* = 125 °C and *TB* = 25 °C

In this situation, the contact pressure increases with the increase of applied force after 1 kN. The maximum contact pressure remained constant for the remaining forces. However, the contact width increases with the increase of the applied force. Figure 8(a) shows the variation of the contact pressure as a function of the contact width. It can be seen that, when the applied force exceeds 10 kN, the contact pressure reached a constant maximum value. The increase of contact width is almost linear to the applied force, fig. 8(b).

In order to analyze the effect of the temperature on the contact state, a different boundary of temperature, *TA* and a fixed value of *TB* (25 °C) were adopted. The force of 10 kN was applied. It can be seen that, variation of *TA* has a great effect on contact behavior as shown in fig. 9. Besides, the contact width has a significant effect on the heat transfer and increases with the increase of *TA*. This effect is also obvious on plastic strain contours, fig. 10.

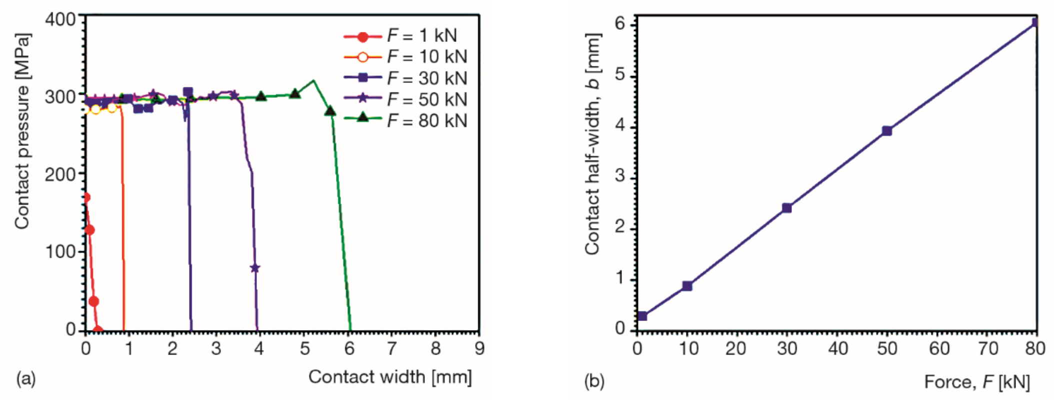

Figure 8. Thermomechanical elastic-plastic for *TA* = 125 °C and *TB* = 25 °C; (a) variation of contact pressure along half-contact and (b) contact width *vs.* applied force

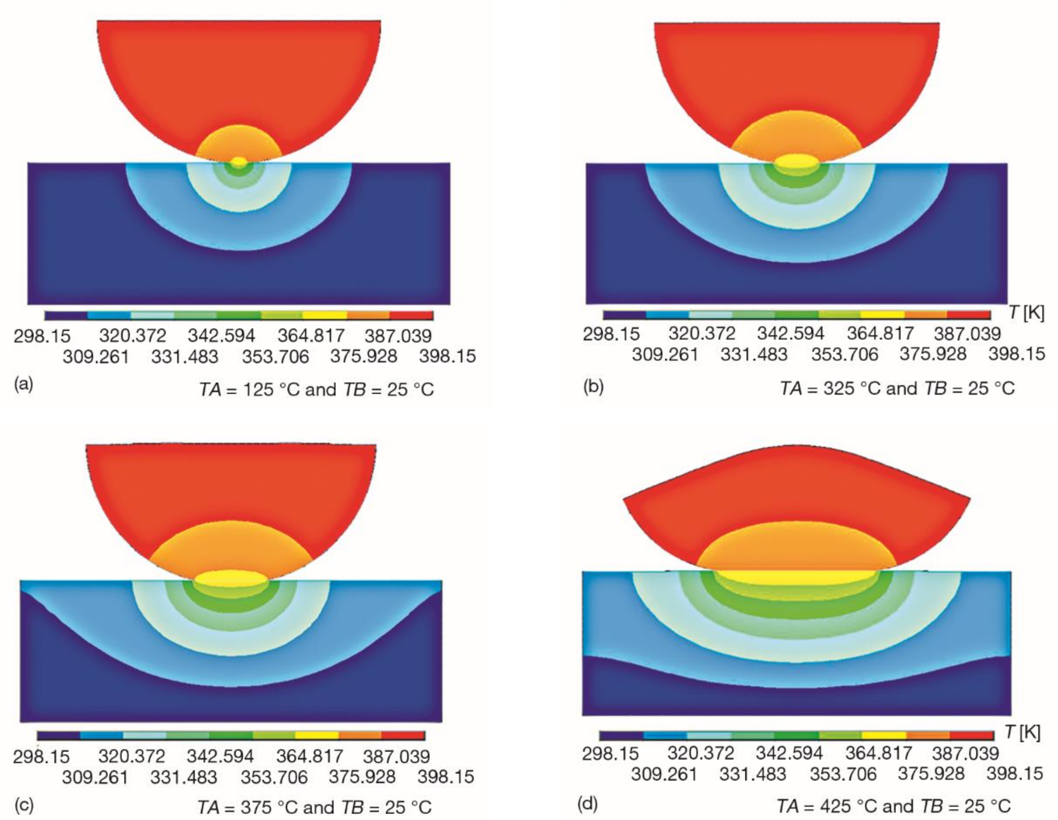

Figure 9. Temperature contours with different temperature gradients and *F* = 10 kN

Furthermore, fig. 11 presents the variation of other contact parameters with *TA* variation. The contact pressure decreases with the increase of the temperature *TA*, fig. 11(a). This is due to the fact that an aluminum cylinder reaches the plastic regime faster with higher temperature as compared to the lower temperature. In addition, the variation of contact width is presented in fig. 11(b). The contact width increases with the increase of *TA* especially for high temperature situations.

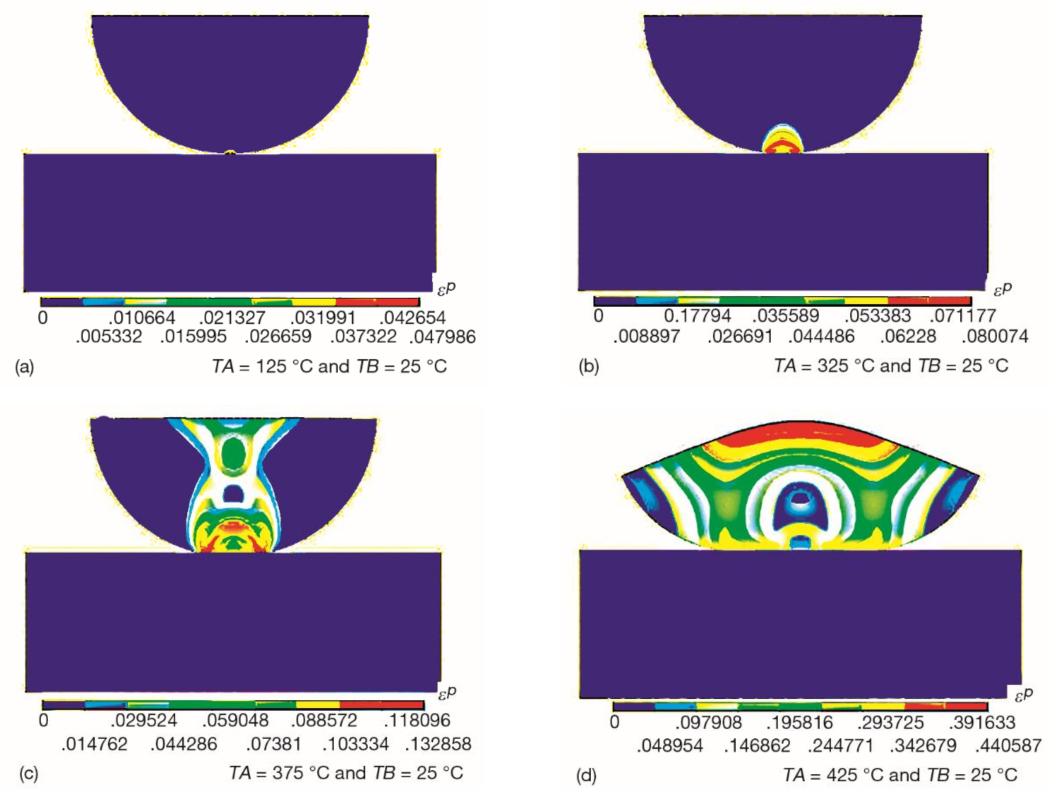

Figure 10. Plastic strain contours with different temperature gradients and *F* = 10 kN

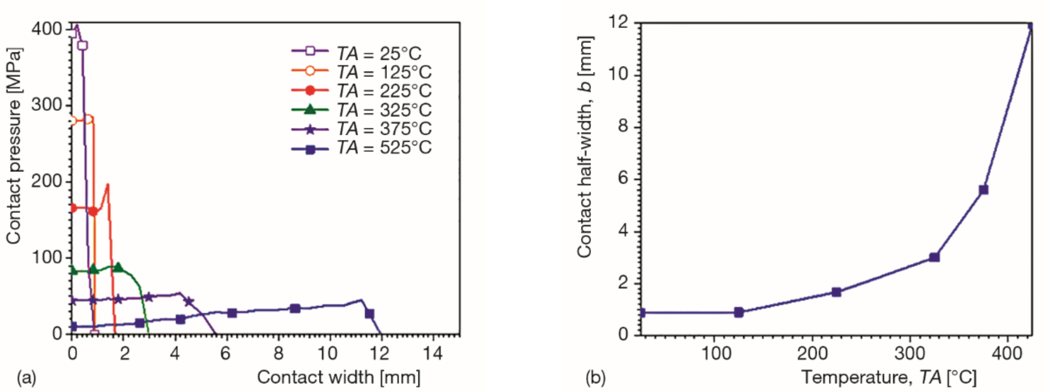

Figure 11. Thermomechanical elastic-plastic contact for *TB* = 25 °C and different *TA* with *F* = 10 kN; (a) variation of contact pressure along half-contact and (b) contact width *vs.* *TA*

Conclusion

In this study, a thermomechanical model has been improved to investigate the thermal effect on the contact with elastic-plastic behavior. A coupled finite element formulation was employed using ANSYS code. Firstly, the model was compared to other works done by previous researchers on elastic-plastic contact problem with thermal effects. At the beginning, an elastic-plastic contact problem without thermal effects was compared to other works done by previous researchers. Secondly, this model was compared with an elastic-plastic contact problem with thermal effects, which solves thermomechanical equations using a *TCC* function of temperature and contact pressure, and a coupled finite element of ANSYS PLANE 223¸ when all the thermal and mechanical parameters of the material depend of the temperature. Next, the effects of different applied forces and different temperature of the aluminum cylinder were analyzed. It has been found that, the high-applied forces influence the improvement of the heat transfer between the two bodies in contact. Besides, there is a great variation in contact features due to the variation of material properties resulting from heat transfer in the aluminum cylinder. As a result, the cylinder is subjected to a high deformation.

Finally, the addition of the phase changes in this thermomechanical model can be addressed in future work.

Acknowledgment

We would like to acknowledge the DGRSDT- MESRS of Algeria, the CEGeoG-Tech, UNIMAP Perlis, of Malaysia for their supports of this study.

Nomenclature

b – width (radius) of the contact, [m]
E^* – equivalent elastic modulus, [Pa]
F – force, [N]
P – pressure, [Pa]
P_C – contact pressure, [Pa]
P_0 – pressure located at center point, [Pa]
TA – temperature of the plate at the top surface, [K]
TB – temperature of the plate at bottom surface, [K]
T_C – contact temperature, [K]
TCC – thermal contact conductance, [$\mathrm{Wm^{-2}k^{-1}}$]

References

[1] Johnson, K. L., *Contact Mechanics,* Cambridge Press, Cambridge, UK, 1985
[2] Dandagwhal, R. D., Kalyankar V. D., Design Optimization of Rolling Element Bearings Using Advanced Optimization Technique, *Arab J. Sci. Eng., 44* (2019), 9, pp. 7407-7422
[3] Rodriguez-Tembleque, L., Aliabadi, M., Indentation Response of Piezoelectric Films Under Frictional Contact, *International Journal of Engineering Science, 107* (2016), Oct., pp. 36-53
[4] Hao, G., Liu, Z., Thermal Contact Resistance Enhancement with Aluminum Oxide Layer Generated on TiAlN-Coated Tool and Its Effect on Cutting Performance for H13 Hardened Steel, *Surface & Coatings Technology, 385* (2020), Mar., 125436
[5] Ma, C., *et al.*, Thermal Contact Conductance Modeling of Baring Outer Ring/Bearing Housing Interface, *International Journal of Heat and Mass Transfer, 150* (2020), Apr., 119301
[6] Ma, C., *et al.*, Simulation and Experimental Study on the Thermally Induced Deformations of High-Speed Spindle System, *Applied Thermal Engineering, 86* (2015), July, pp. 251-268
[7] Liu, J., *et al.*, Thermal Contact Conductance between Rollers and Bearing Rings, *International Journal of Thermal Sciences, 147* (2020), Jan., pp. 106-140
[8] Tobias Hultqvista, T., *et al.*, Larsson, R., Transient Analyzis of Surface Roughness Features in Thermal Elastohydrodynamic Contacts, *Tribology International, 141* (2020), Jan., 105915
[9] Shahzamanian, M. M., *et al.*, Transient and Thermal Contact Analyzis for the Elastic Behavior of Functionally Graded Brake Disks Due to Mechanical and Thermal Loads, *Materials and Design, 31* (2010), 10, pp. 4655-4665
[10] Wang, L., *et al.*, Characteristics of the Friction Between Aluminum and Steel at Elevated Temperatures During Ball-on-Disc Tests, *Tribology letters, 36* (2009), Jan., pp. 183-190

[11] Huttunen-Saarivirta, E., *et al.*, Wear of Additively Manufactured Tool Steel in Contact with Aluminum Alloy, *Wear, 432-433* (2019), Aug., 202934
[12] Tarasov, S. Yu., *et al.*, Adhesion Transfer in Sliding a Steel Ball Against an Aluminum Alloy, *Tribology International, 115* (2017), Nov., pp. 191-198
[13] Abou Gharam, A., *et al.*, High Temperature Tribological Behavior of Carbon Based (B4C and DLC) Coating in Sliding with Aluminum, *Thin Solid Films, 519* (2010), 5, pp. 1611-1617
[14] Fatoui, K., *et al.*, Simulation of the Thermal History and Induced Mechanical Stresses During a Plasma Spray Coating Process, *Phys. Chem. News., 40* (2008), Mar., pp. 23-28
[15] Chanda, T., Zhou, *et al.*, 3D FEM of the Thermal Events During AA6061 Aluminum Extrusion, *Scr. Mater, 41* (1999), 2, pp. 195-202
[16] Riahi, A. R., *et al.*, Experimental Study of the Disturbed Layer Generation During Hot Rolling Contact of Aluminum with Steel, *Tribology International, 54* (2012), Oct., pp. 42-50
[17] Caprioli, S., Short Rolling Contact Fatigue and Thermal Cracks Under Frictional Rolling – A Comparison Through Simulations, *Engineering Fracture Mechanics, 141* (2015), June, pp. 260-273
[18] Tiberkak, R., *et al.*, Effect of Crack on the Impact of Plates by the Extended Finite Element Method (X-FEM), *J. Mech. Sci. Technol., 28* (2014), 6, pp. 2243-2252
[19] Bian, W., *et al.*, Thermo-Mechanical Analyzis of Angular Contact Ball Bearing, *J. Mech. Sci. Technol, 30* (2016),1, pp. 297-306
[20] Wang, J., *et al.*, Analyzis of Al-Steel Resistance Spot Welding Process by Developing a Fully Coupled Multi-Physics Simulation Model, *Int. J. Heat Mass. Tran., 89* (2015), Oct., pp. 1061-1072
[21] Botto, D., Lavella, M., A Numerical Method to Solve the Normal and Tangential Contact Problem of Elastic Bodies, *Wear, 330-331* (2015), May-June, pp. 629-635
[22] Hertz, H., Ueber die Beruhrung Fester Etastischerkorper, *J. Reine. Angew. Math., 1882* (1982), 92, pp. 156-171
[23] Dongwoo, S., *et al.*, Extended JKR Theory on Adhesive Contact Between Elastic Coatings on Rigid Cylinders Under Plane Strain, *International Journal of Solids and Structures, 71* (2015), Oct., pp. 244-254
[24] Chudzikiewicz, A., Myslinski, A., Thermoelastic Wheel-Rail Contact Problem with Elastic Graded Materials, *Wear, 271* (2011), 1-2, pp. 417-425
[25] Roy, A., Contact Problem in Elasticity, in: *Part of the Springer Proc. In Mathe. and Statistics*, *Aplied Mathematics,* Springer, New York, USA, 2015, vol. 46, pp. 115-124
[26] Chen, X. W., Yue, Z. Q., Non-linear Contact force Law for Spherical Indentation of FGM Coated Elastic Substrate: An Extension of Hertz's Solution, *Int. J. Solids Struct, 191-192* (2020), May, pp. 550-565
[27] Obodan, N. I., *et al.*, Contact Problem for a Rigid Punch and an Elastic Half Space as an Inverse Problem, *J. Math. Sci., 240* (2019), 2, pp. 184-193
[28] Alexandrov V. M., Pozharskii D. A., Three-Dimensional Contact Problems, in: *Solide Mechanics and Aplications,* Springer Science & Business Media, Kluwer Academic Publisher, Boston, Mass., USA, 2001, Vol. 93
[29] Frerot, L., *et al.*, A Fourier-Accelerated Volume Integral Method for Elastoplastic Contact, *Comput. Methods Appl., Mech. Engrg., 351* (2019), July, pp. 951-976
[30] Benramoul, L., Abdellah el-hadj, A., An Elastic-Perfectly Plastic Model for Simulating an Aluminum Particle Behavior During Plasma Thermal Spraying Using the Finite Element Method, *Appl. Surf. Sci, 258* (2011), 2, pp. 962-971
[31] Doca, T., *et al.*, A Frictional Mortar Contact Approach for the Analyzis of Large Inelastic Deformation Problems, *Int. J. Solids Struc, 51* (2014), 9, pp. 1697-1715
[32] Doca, T., Andrade Pires, F. M., Analyzis of a Cylinder-to-Flat Contact Problem at Finite Elasto-Plastic Strains, *Tribol. Int., 79* (2014), Nov., pp. 92-98
[33] Byung, C. L., Byung M. K.., A Computational Method for Elasto-Plastic Contact Problems, *Comput. Struct., 18* (1984), 5, pp. 757-765
[34] Jamari, J., Schipper, D. J., An Elastic-Plastic Contact Model of Ellipsoid Bodies, *Tribol. Lett., 21* (2006), 3, pp. 262-271
[35] Ghaednia, H., *et al.*, A Review of Elastic-Plastic Contact Mechanics, *Appl.Mech.Rev, 69* (2017), 6, 060804
[36] Zhu, H., *et al.*, An Elastic-Plastic Contact Model for Line Contact Structures, *Sci. China Phys. Mech. Astron., 61* (2018), 5, 054611
[37] Feldhacker, J., *et al.*, Strength Assessment of a Pressurized Thick-Walled Cylinder Using Structural-Thermal Coupled Finite Element Analyzis, *IMECE2007*, (2007), May, pp. 171-177

[38] Chbiki, M., *et al.,* Thermal Effect of the Thermomechanical Behavior of Contacts in a Traveling Wave Tube, *Thermal science*, *20* (2016), 6, pp. 1983-1990
[39] Bahrami, M., Culham, R., Thermal Contact Resistance at Low Contact Pressure: Effect of Elastic Deformation, *International Journal of Heat and Mass Transfer, 48* (2005), 16, pp. 3284-3293
[40] Danouni, S., *et al.*, A Thermo-Mechanical Analyzis of a Particle Impact During Thermal Spraying, *Appl. Surf. Sc.i, 371* (2016), May, pp. 213-223
[41] Heydari, A., Elasto-Plastic Analyzis of Cylindrical Vessel with Arbitrary Material Gradation Subjected to Thermo-Mechanical Loading *via* DTM, *Arab. J. Sci. Eng., 44* (2019), 10, pp. 8875-8891
[42] Madhusudana, C. V., *Thermal Contact Conductance*, 2nd ed., Springer, New York, USA, 2014
[43] Liu, Y., *et al.,* Effect of Contact Pressure and Interface Temperature on Thermal Contact Resistance between 2Cr12NiMoWV/BH137 and γ-TiAl/2Cr12NiMoWV Interfaces, *Thermal Science*, *24* (2020), 1A, pp. 313-324
[44] ***, Theory Reference Guide, Mechanical Apdl, *Ansys. Inc.,* 2012
[45] ***, Contact Technology Guide, *Ansys. Inc.,* 2012

Paper submitted: October 26, 2020
Paper revised: July 30 2021
Paper accepted: August 16, 2021